AT&T Technical Journal
Vol. 64, No. 8, October 1985
Printed in U.S.A.

Performance Comparison of InGaAsP Lasers Emitting at 1.3 and 1.55 μm for Lightwave System Applications

By N. K. DUTTA,* R. B. WILSON,† D. P. WILT,* P. BESOMI,‡ R. L. BROWN,* R. J. NELSON,† and R. W. DIXON*

(Manuscript received April 11, 1985)

Experimental results relative to the performances of real index-guided InGaAsP lasers emitting near 1.3 and 1.55 μm are described and compared. The laser structures discussed are the etched mesa buried heterostructure, channeled substrate buried heterostructure, and the double channel planar buried heterostructure. The effect of Auger recombination and intervalence band absorption on the threshold current and external differential quantum efficiency is discussed. The effect of the larger Auger coefficient at 1.55 μm is compensated by a lower carrier density at threshold at 1.55 μm so that the total nonradiative current loss for lasers emitting at 1.55 μm is not significantly larger than that for lasers emitting at 1.3 μm. A small linear shunt leakage current (~10 mA) can increase the T_0 to ~100K. We report threshold currents as low as 11 and 15 mA (at 30°C) and continuous-wave operating temperatures as high as 130 and 110°C for lasers emitting at 1.3 and 1.55 μm, respectively.

I. INTRODUCTION

Lightwave transmission systems are being installed throughout the world at a rapidly escalating pace. These new systems offer higher bit rate and longer repeater spacing than conventional systems and thus reduce the transmission cost per bit.[1]

* AT&T Bell Laboratories. † Lytel, Inc., Somerville, New Jersey. ‡ General Optronics, Edison, New Jersey.

Most of the lightwave systems installed so far (often called first-generation systems) use multimode fibers and an operating wavelength of about 0.85 μm.[2] Second-generation systems using single-mode fibers and an operating wavelength near 1.3 μm offer longer repeater spacings because the loss of silica fibers is lower at 1.3 μm than at 0.85 μm.[2,3] Zero chromatic dispersion near 1.3 μm for silica fibers allows the use of multimode laser sources in single-mode fibers for long-distance high bit-rate transmission without significant dispersion penalty.[2,3] Although the full potential of lightwave systems operating at 1.3 μm has not yet been realized because it is a relatively new technology, it is quite conceivable that a third-generation system operating at 1.55 μm may be extensively installed in the near future because the silica fiber loss is minimum at 1.55 μm.[4] Laboratory experiments have already demonstrated the high system performance that can be achieved at this wavelength.[5,6]

Development and subsequent installation of new lightwave systems have been driven by the development of new high-quality components, namely fibers, sources (lasers), detectors (avalanche photodiode or pin photodiode), or integrated front ends, and transmitter and receiver electronics. For example, the development of low-cost silica fibers with zero dispersion at 1.55 μm will certainly influence the third-generation systems. High-speed integrated circuits for receiver and transmitter packages are currently being developed for high bit-rate (>1 Gb/s) systems. This paper compares the performance of InGaAsP lasers emitting at 1.3 and 1.55 μm. The former is currently in use in several second-generation systems and the latter can be a single-frequency source for third-generation systems operating at that wavelength using conventional single-mode silica fibers.

The performance requirements for lasers used in lightwave transmitters usually include linear (kink-free) light-current characteristics up to a certain power output (typically ~5-mW/facet, ~0-dBm power input to the fiber), capability of high bit-rate modulation, and long operating life. Low-threshold and high-differential quantum efficiency are desirable (necessary for some systems) in order to reduce the bias current and modulation needed from the drive circuitry. Since most lightwave transmitters need to operate over a range of temperature, a weak temperature dependence of the threshold of the laser is desirable—otherwise, thermoelectric controllers are required inside the transmitter package in order to stabilize the laser temperature. The conventional InGaAsP double heterostructure laser emitting at 1.55 μm may be more sensitive to temperature and have lower differential quantum efficiency than a laser emitting at 1.3 μm. The former is due to larger nonradiative Auger recombination rate[7,8] and the latter may be due to larger intervalence band absorption[8,9] at longer wavelengths.

The effect of these processes is discussed in detail in Sections II and III. We find that the effect of the larger Auger coefficient at 1.55 μm is compensated by smaller carrier density at threshold so that the nonradiative Auger current at 1.55 μm is not significantly larger than that for 1.3 μm.

The fabrication of InGaAsP lasers emitting at 1.55 μm by Liquid Phase Epitaxy (LPE) usually requires the growth of an additional InGaAsP layer (antimeltback layer) in order to prevent the meltback of the active layer in subsequent growth of InP layer.[10]

The effect of the thickness of this antimeltback layer on threshold current and efficiency of 1.55-μm lasers is discussed in Section IV. Although this layer need not be present when the double heterostructure is grown by Vapor Phase Epitaxy (VPE), fabrication of Distributed Feedback (DFB)-type single-frequency lasers usually requires an intermediate band gap layer (1.1 to 1.3 μm) between the active layer (1.55 μm) and InP layers. Antimeltback layers are not needed for 1.3-μm InGaAsP double heterostructures grown by LPE, although DFB lasers emitting at 1.3 μm need an intermediate gap layer (~1.1 μm) between the active layer and the InP cladding layers for optimization.

Real index-guided lasers are needed as sources for high-performance fiber communication systems because these lasers are less susceptible to light-current nonlinearities and intensity self-pulsations than gain-guided lasers.[11] Many strongly index-guided laser structures utilize reverse biased junctions for current confinement. Leakage currents, that is, current flowing around the active region, may be responsible for high-threshold and light-current sublinearity in nonoptimized structures.[12] Since the leakage currents in many cases varies as $\exp(\Delta E_g/kT)$, where ΔE_g is the difference in band gap of the blocking layers (InP) and the active region (1.3- or 1.55-μm InGaAsP), we expect the leakage currents in 1.55-μm InGaAsP lasers to be smaller than those in 1.3-μm InGaAsP lasers. This is discussed in Section V.

Experimental results from several types of real index-guided lasers emitting at 1.3 and 1.55 μm are compared in Section VI. These results show that the 1.55-μm lasers have somewhat higher threshold current (~30 percent at 30°C) and lower light output at 100 mA (~40 percent at 30°C). The former, in our opinion, is due principally to smaller mode confinement factor (because of the presence of antimeltback layer), and the latter is due to the combined effect of lower photon energy (~20 percent) and larger intervalence band absorption and free carrier absorption at 1.55 μm. The measured threshold current as a function of temperature for lasers emitting at both wavelengths can be represented by the expression $I_{th} \sim I_0 \exp(T/T_0)$, where T_0 is a parameter determining the temperature sensitivity. Similar T_0 values are observed for lasers emitting at both wavelengths except in cases

where leakage current is believed to affect T_0. The limitations in high bit-rate long-haul fiber communication systems introduced by the source linewidth are discussed in Section VII.

II. AUGER EFFECT

Since the initial work by Beattie and Landsberg,[13] it has been established that the band-to-band Auger processes are often a major nonradiative carrier loss mechanism in small band gap semiconductors. We expect the nonradiative Auger rate for 1.55-μm band gap material to be larger than that for 1.3-μm material.

The Auger rate (R_a) in undoped semiconductor varies approximately as

$$R_a = \gamma n^3, \tag{1}$$

where γ is the Auger coefficient and n is the injected carrier density.[13] The radiative recombination rate varies approximately as

$$R_r = Bn^2, \tag{2}$$

where B is the radiative recombination coefficient.[14,15] The current density of a broad-area laser at lasing threshold (in the absence of other recombination mechanisms) is given by

$$\begin{aligned} J &= eR_r d + eR_a d \\ &= J_r + J_a, \end{aligned} \tag{3}$$

where e is the electron charge and d is the active layer thickness, J_r, J_a are the radiative and the Auger component of the current, respectively. The Auger coefficient γ in eq. (1) is dominated by phonon-assisted Auger processes for larger band gap semiconductors and by band-to-band processes for small band gap semiconductors. Detailed discussion of band-to-band, phonon-assisted, and trap Auger processes in direct gap semiconductors are given in Ref. 7. Figure 1 shows the calculated γ for InGaAsP alloy lattice matched to InP for $n = 10^{18}$ cm^{-3}. Because of the uncertainty in the calculation of the absolute magnitude of the Auger coefficient, we have plotted γ in Fig. 1 normalized to its value (γ_0) for 1.3-μm InGaAsP. The calculated γ_0 $\sim 1 \times 10^{-28}$ cm^6 sec^{-1}. The measured values by several authors are shown in Table I. Figure 1 shows that the Auger coefficient for 1.55-μm InGaAsP is about a factor of 4 larger than that for 1.3-μm InGaAsP. Agrawal and Dutta[20] have found that the Auger coefficient for 1.55-μm InGaAsP is about a factor of 3 larger than that for 1.3-μm InGaAsP from an analysis of threshold current of stripe geometry InGaAsP lasers emitting at 1.3 and 1.55 μm. Thus the Auger coefficient for 1.55-μm InGaAsP is about 3 to 4 times larger than that for 1.3-μm InGaAsP.

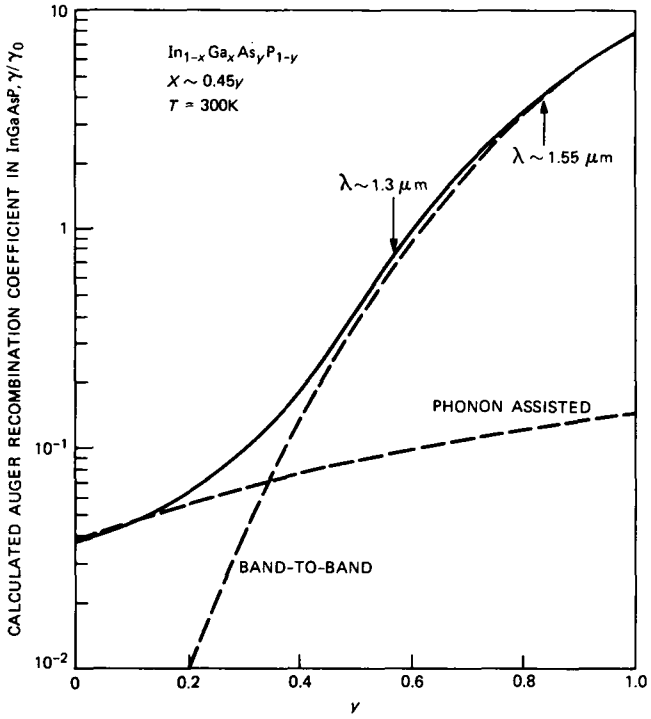

Fig. 1—The relative Auger coefficient γ/γ_0 is plotted as a function of band gap of InGaAsP.

Table I—Measured Auger coefficients

(cm^6sec^{-1})	Reference	Comment
5×10^{-29} (CCHS)	Mozer et al. (1982)[16]	$\lambda = 1.3\ \mu m$
$2.3 \pm 1 \times 10^{-29}$ (Total)	Sermage et al. (1983)[17]	$\lambda = 1.3\ \mu m$, optically pumped
1×10^{-29} (Total)	Henry et al. (1981)	$\lambda = 1.3\ \mu m$, doping dependence of τ
$<3 \times 10^{-29}$ (Total)	Su et al. (1982)	$\lambda = 1.3\ \mu m$
3×10^{-29} (Total)	Thompson (1983)[18]	Fit to data of Su et al.
$3\text{–}8 \times 10^{-29}$ (Total)	Uji (1983)[19]	$\lambda = 1.3\ \mu m$ LEDs
$2.8\text{–}1.5 \times 10^{-29}$	Wintner and Ippen (1984)	$\lambda = 1.3\ \mu m$ optically pumped
7.5×10^{-29}	Wintner and Ippen (1984)	$\lambda = 1.55\ \mu m$ optically pumped

The radiative recombination rate B can be calculated by using the Gaussian Halperin-Lax band tails and Stern's matrix elements.[14,15] Figure 2 shows the calculated B/B_0 for InGaAsP for $n = 10^{18}$ cm^{-3}. B_0 is the value of B for 1.3-μm InGaAsP. The calculated $B_0 = 1 \times 10^{-10}$ cm^3 sec^{-1}. The measured values lie in the range $0.9\text{–}1.5 \times 10^{-10}$ cm^3 sec^{-1}.[21,22] Equations (1) and (2) are strictly valid only for nondegenerate electron and hole gas. However, at high injected carrier densities ($\sim 2 \times 10^{18}$ cm^{-3}) at laser threshold the electron and holes are degen-

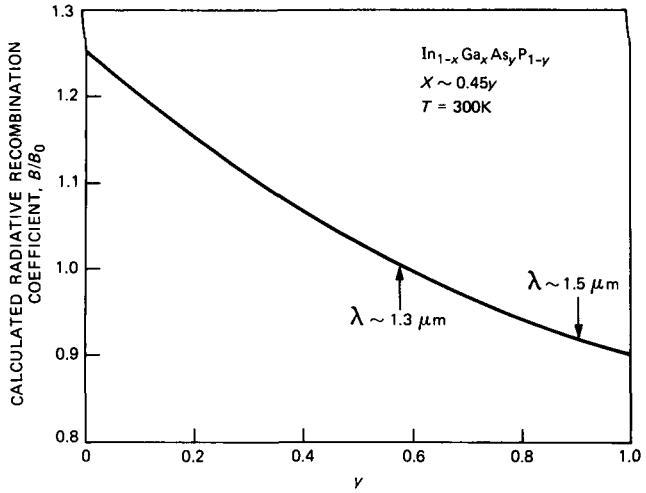

Fig. 2—The relative radiative recombination coefficient B/B_0 is plotted as a function of band gap of InGaAsP.

erate. Degeneracy effects can be introduced by writing γ, B as functions of n. Both γ and B decrease slowly with increasing carrier density.[7,8,14,15]

The laser threshold currents are determined principally by the magnitudes of γ, B, and the threshold carrier density. The latter depends to some extent on the laser structure, for example, through the mode confinement factor and optical absorption. However, it is possible to determine the injected carrier density at transparency (n_0) from the band structure parameters alone.[23] We consider undoped materials. Using the Joyce-Dixon approximation[24] for the quasi-Fermi levels and assuming parabolic bands, we show the calculated n_0 for InGaAsP in Fig. 3. The threshold carrier density is usually 30 to 40 percent higher than n_0. Note that n_0 for 1.55-μm InGaAsP (in Fig. 3) is smaller than that for 1.3-μm InGaAsP. This is due to smaller conduction band effective mass at long wavelengths. Since the radiative recombination current varies as Bn^2, Figs. 2 and 3 suggest that the threshold current of 1.55-μm InGaAsP lasers should be lower than that for 1.3-μm InGaAsP lasers in the absence of Auger recombination. This is shown in Fig. 4c.

Figure 4 shows the calculated radiative and Auger components of the current, plotted as a function of temperature, for 1.3- and 1.55-μm InGaAsP-InP broad-area double heterostructure lasers. The radiative component is calculated using a constant (temperature-independent) absorption loss of 30 cm^{-1} in the active layer as in Ref. 7. The Auger component of the total current is calculated using eq. (1) for Auger

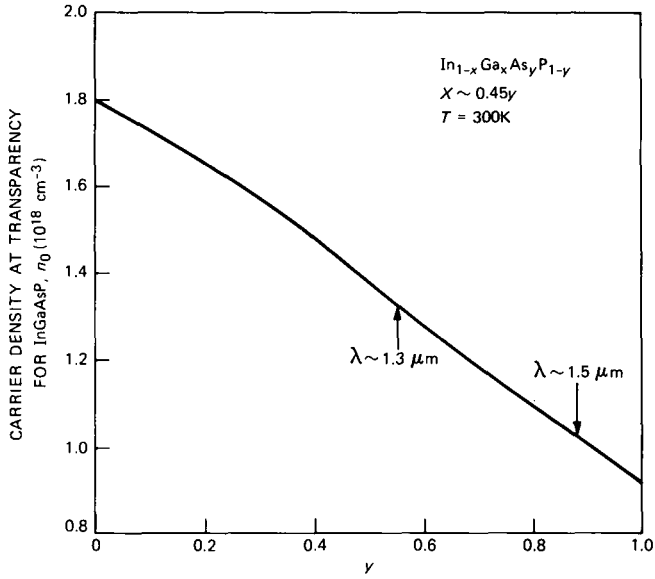

Fig. 3—The injected carrier density at transparency for undoped InGaAsP.

recombination rate, the temperature dependence of threshold carrier density (n_{th}) from Figs. 17 and 23 of Ref. 7, the calculated temperature dependence of γ, and $\gamma_0 = 3 \times 10^{-29}$ cm^6 sec^{-1} (which falls within the range of the measured values but is smaller than the calculated value[7] of 1×10^{-28} cm^6 sec^{-1}).

Auger rate calculations using the Kane band model[25] result in Auger coefficients higher than observed experimentally.[7,8] Recently, Haug[26] has calculated the Auger coefficients in 1.3-μm InGaAsP using the band model of Chelikowsky and Cohen[27] for InP but with an energy gap assumed to be that of γ = 1.3-μm InGaAsP. He finds that the phonon-assisted Auger processes (CCCHP[7]) are dominant with a value of $\sim 2.5 \times 10^{-29}$ cm^6 sec^{-1}. Using a calculated temperature dependence of the phonon-assisted Auger process, this would result in a T_0 value of 100 to 110K for 1.3-μm InGaAsP-InP lasers, which is higher than the observed value in broad-area lasers (~60 to 70K). There is sufficient uncertainty in the band structure parameters and the carrier concentration at threshold that it is unreasonable to expect better agreement between calculation and experiment. Figure 5 shows the predicted T_0 values (between 300 and 350K) plotted as a function of Auger coefficient (at 300K) for two different values of carrier density at threshold. The quantity k is the ratio of the Auger coefficients at 350 and 300K. The smaller value is the calculated result for the phonon-assisted Auger processes, and the higher value is that for the band-to-band processes. Although the temperature dependence of γ

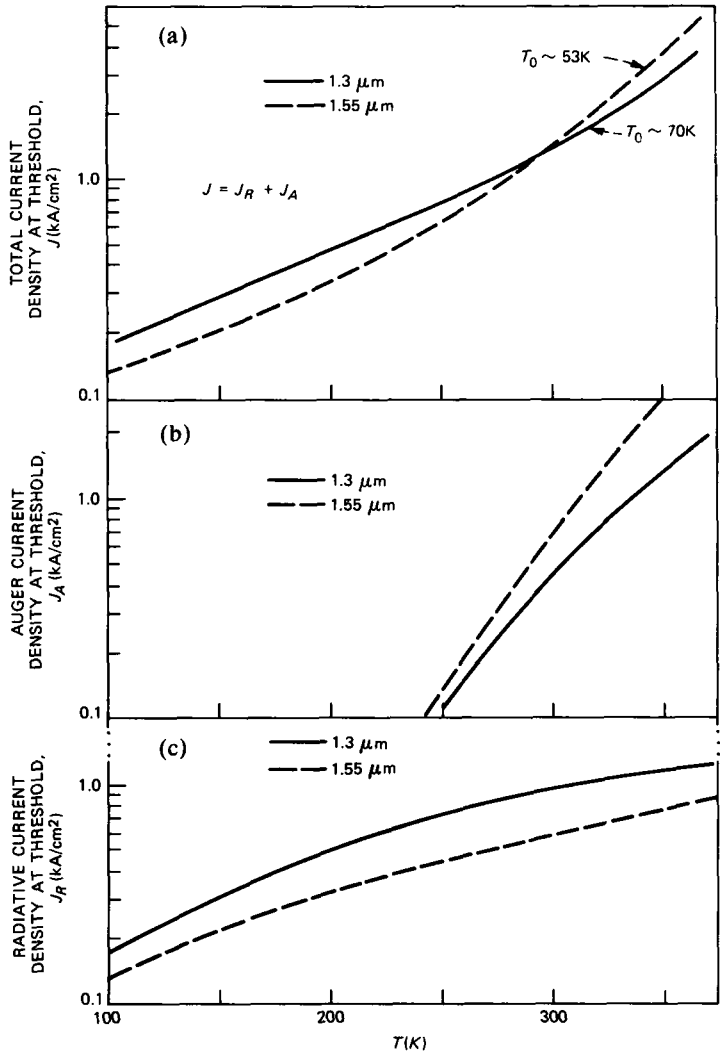

Fig. 4—The calculated radiative and Auger component of the current for lasers emitting at 1.3 and 1.55 μm. (a) Radiative. (b) Auger component. (c) Total.

has not been experimentally determined, the calculated temperature dependence of n_{th} agrees well with that of the measured threshold current using short pulses.[28] The total threshold current which is the sum of the radiative and Auger component is shown in Fig. 4a. The smaller J_R for 1.55-μm lasers is approximately compensated by the larger J_A. The above calculation is for an InGaAsP active layer with InP cladding layers both for 1.3- and 1.55-μm lasers. The presence of an antimeltback layer reduces the confinement factor, which increases

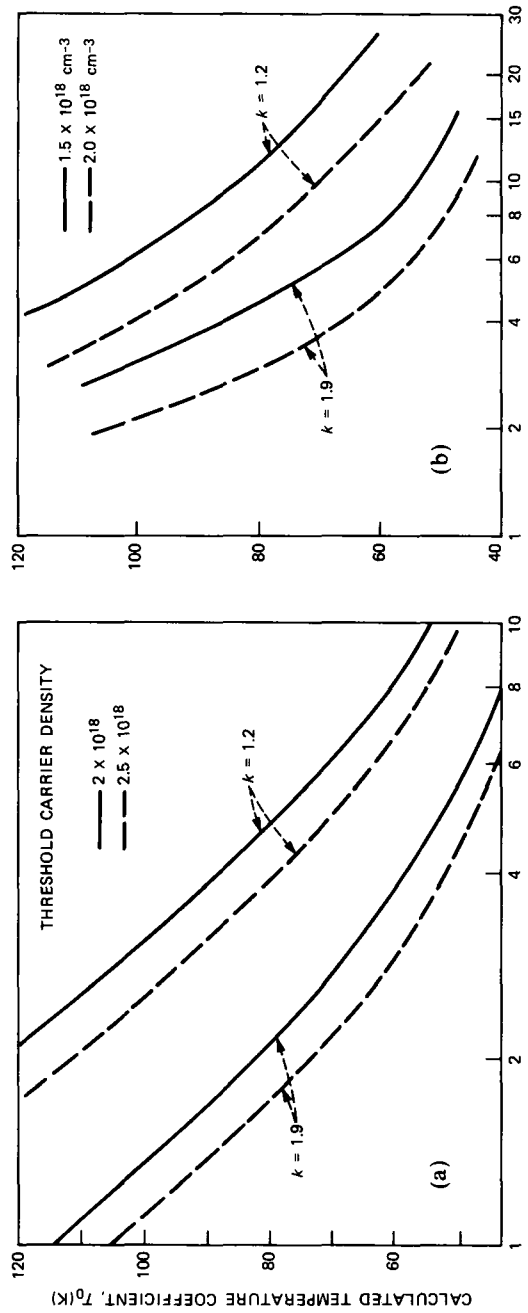

Fig. 5—The calculated T_0 values as a function of Auger coefficient. (a) $\lambda = 1.3$-μm InGaAsP. (b) $\lambda = 1.55$-μm InGaAsP.

the threshold current of 1.55-μm lasers over that shown in Fig. 4. This is discussed in detail in Section IV. Furthermore, heterobarrier leakage due to drift and diffusion may be responsible for increased threshold current of 1.3-μm InGaAsP DH lasers if the p-cladding layer doping is too low.[29,30] These lasers also exhibit a higher temperature dependence of threshold (lower T_0) than is commonly observed. Such heterobarrier leakage is smaller in 1.55-μm InGaAsP lasers because of larger barrier height. The high-energy electrons generated in the Auger process may also escape (thermionic emission) over the heterobarrier, in which case the carrier leakage is expected to be independent of the barrier height and p-cladding doping. Shah et al.[31] have reported observation of hot carriers, and Yamakoshi et al.[32] have reported observation of carrier leakage in 1.3-μm InGaAsP-InP lasers. However, Henry et al.[33] did not observe hot carriers in their experiments.

III. INTERVALENCE BAND ABSORPTION

Intervalence band absorption is an optical loss mechanism in the active region of InGaAsP lasers that can reduce the external differential quantum efficiency.[8,9] The external differential quantum efficiency (η_d) is given approximately by

$$\eta_d = \frac{\alpha_m}{\alpha_m + \alpha}, \tag{4}$$

where

$$\alpha = \Gamma\alpha_a + (1 - \Gamma)\alpha_c,$$

where α_m is the mirror loss, Γ is the confinement factor, and α_a and α_c are the absorption and cladding layer losses, respectively. For a 250-μm long laser the "equivalent distributed" loss $\alpha_m \simeq 40$ cm^{-1} using R = 0.35. Figure 6 shows η_d plotted as a function of α_a for several values of Γ. We assume $\alpha_c = 30$ cm^{-1}. The light output L at a current ΔI above threshold is given by $L = \eta_d E_g \Delta I$, where E_g is the band gap of the active layer. The light output from 1.55-μm lasers for a given ΔI and η_d is lower than that for 1.3-μm lasers because the former has lower photon energy.

Sugimura[8] has calculated the intervalence band absorption in III–V semiconductors using Kane band model. The absorption is larger for small band gap semiconductors and increases with increasing temperature. The calculated absorption (α) normalized to its value (α_0) for 1.3-μm InGaAsP at 300K is shown in Fig. 7. The calculated α_0 is approximately 30 cm^{-1}. Henry et al.[34] have extrapolated the intervalence band absorption in 1.55-μm InGaAsP from measurements in InGaAs. Adams et al.[9] have proposed that the high temperature

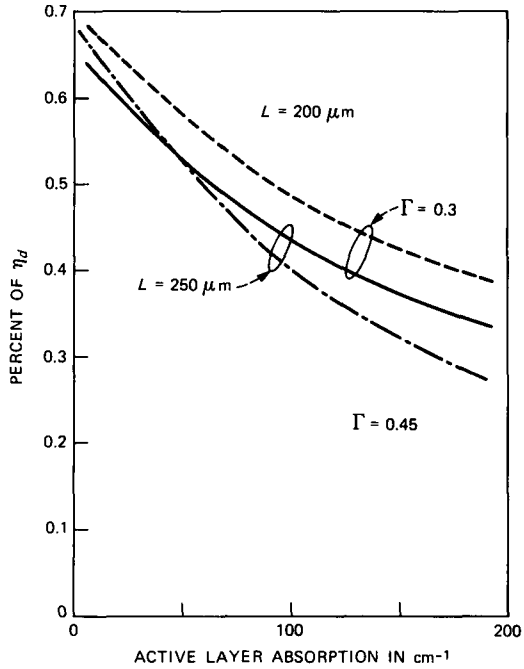

Fig. 6—The calculated external differential quantum efficiency as a function of optical loss in the active.

sensitivity of threshold (low T_0) current of 1.6-μm InGaAsP lasers is due to intervalence band absorption. Although this is not the dominant mechanism responsible for low T_0 of 1.55-μm InGaAsP lasers, it may be why the observed η_d of InGaAsP lasers emitting at 1.55 μm is lower than that for lasers emitting at 1.3 μm.

IV. ANTIMELTBACK THICKNESS

Both 1.3- and 1.55-μm InGaAsP double heterostructures have been grown by LPE and VPE techniques. However, as mentioned previously, for LPE growth it is necessary to grow a short-wavelength (~1.1 to 1.3-μm) InGaAsP layer over the 1.55-μm active layer to prevent meltback of the active layer during the subsequent growth of InP layer. A thick antimeltback layer reduces the confinement factor of the guided mode and hence increases the laser threshold. However, a smaller confinement factor reduces the effect of intervalence band absorption and hence increases the differential quantum efficiency. We now calculate the effect of antimeltback layer thickness on device threshold.

The threshold gain g_{th} is given by

$$\Gamma g_{\text{th}} = \Gamma\alpha_a + (1 - \Gamma)\alpha_c, \tag{5}$$

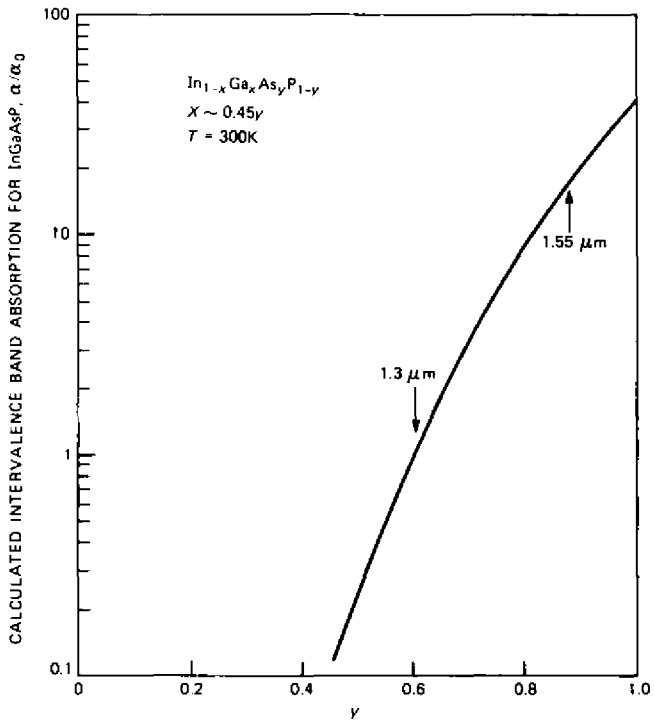

Fig. 7—The calculated intervalence band absorption from Ref. 8 normalized to its value for 1.3 μm.

where Γ, α_a, and α_c are the confinement factor and the absorption in the active and cladding layers, respectively. We assume $\alpha_c = 30$ cm^{-1} and $\alpha_a = 40$ cm^{-1} and 150 cm^{-1} for the curves in Fig. 8. The confinement factor is calculated using the analysis of Butler[35] for a four-layer guide. The refractive index of InP, 1.3-μm InGaAsP, and the 1.55-μm active layer are 3.21, 3.4, and 3.55, respectively. For the calculated g_{th} in eq. (5), the threshold carrier density (n_{th}) is obtained from previous calculations. Then the threshold current density at 300K is obtained using eq. (3) with $B = 0.9 \times 10^{-10}$ cm^{-3} sec^{-1} and $\gamma = 9 \times 10^{-29}$ cm^6 sec^{-1}. Figure 8 shows the results of the calculation for both J_{th} and η_d as a function of antimeltback layer thickness. Thus, both the threshold current and the external differential quantum efficiency increase as the antimeltback layer thickness is increased. The former is due to larger threshold gain caused by reduced confinement factor as the antimeltback layer thickness is increased, and the latter is due to lower loss experienced by the lasing mode in the active layer (in the above mode) due to smaller Γ. The observed smaller η_d of the 1.55-μm lasers may also be due to larger free carrier absorption both in the cladding and active layer at longer wavelengths.

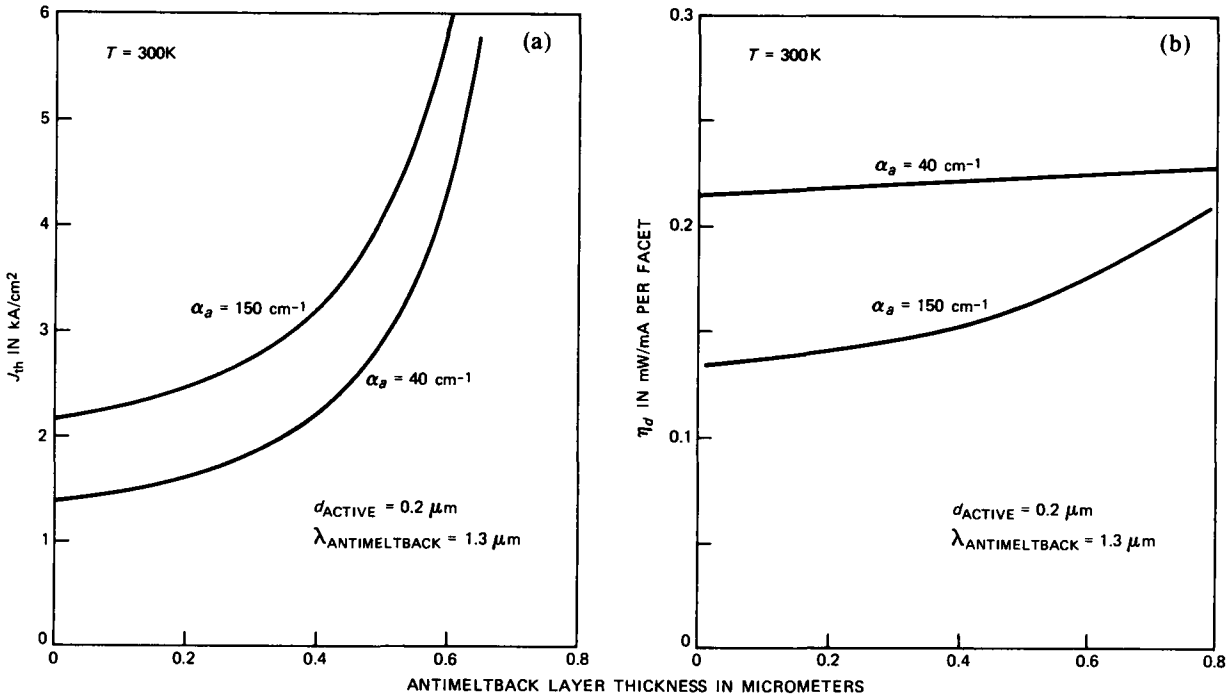

Fig. 8—The (a) threshold current and (b) external differential quantum efficiency as a function of the thickness of the antimeltback layer.

V. LEAKAGE CURRENT

Real index-guided lasers are needed for high bit-rate fiber transmission systems because of their superior performance over gain-guided lasers.[11] Many strongly index-guided lasers utilize reverse biased junctions for current confinement to the active region.[12] It is generally believed that leakage currents, that is, currents flowing around the active region, are responsible for high threshold current, light-current sublinearity, and poor high-temperature performance of nonoptimized laser structures. We have previously analyzed the leakage currents in several 1.3-μm InGaAsP-InP laser structures using electrical equivalent circuit models.[12] The leakage current through leakage paths with pin junctions varies approximately as $\exp(\Delta E_g/kT)$, where ΔE_g is the band gap difference between InP and the active layer. $\Delta E_g \sim 0.39$ eV and ~0.55 eV for InGaAsP lasers emitting at 1.3 and 1.55 μm, respectively. Thus the magnitude of leakage current is expected to be approximately $\sim\exp(0.16\ \text{eV}/kT) \sim e^6$ times smaller for InGaAsP lasers emitting at 1.55 μm than for lasers emitting at 1.3 μm. In many laser structures the leakage current flows through forward-biased pin InP homojunctions.[12] A fraction of this current in 1.3-μm InGaAsP lasers can be detected as radiative emission at ~0.95 μm, which is the band gap of InP.[36] No emission at ~0.95 μm is observed from 1.5-μm InGaAsP lasers, which suggests that leakage currents through InP homojunctions are significantly smaller in these lasers. These considerations do not apply to linear resistive shunt paths.

VI. EXPERIMENTAL RESULTS

In this section, we compare the experimental results from several types of real index-guided InGaAsP lasers emitting at 1.3 and 1.55 μm. We first discuss the strongly index-guided lasers. Over the last few years, we have fabricated the Channeled Substrate Buried Heterostructure (CSBH),[37] the Etched Mesa Buried Heterostructure (EMBH)[38,39] and the Double-Channel Planar Buried Heterostructure (DCPBH)[40] lasers (see Fig. 9).[41] The CSBH laser has a nonplanar active region and can be fabricated using one LPE growth. The EMBH and DCPBH lasers have planar active regions, which make them compatible with the fabrication of DFB and DBR-type single-frequency lasers.[42] These structures need two epitaxial growth steps for fabrication. Schematic cross sections of these laser structures are shown in Fig. 9.

6.1 Double channel planar buried heterostructure lasers

The schematic cross section of this device structure is shown in Fig. 9c. The fabrication of DCPBH lasers involves two epitaxial growth

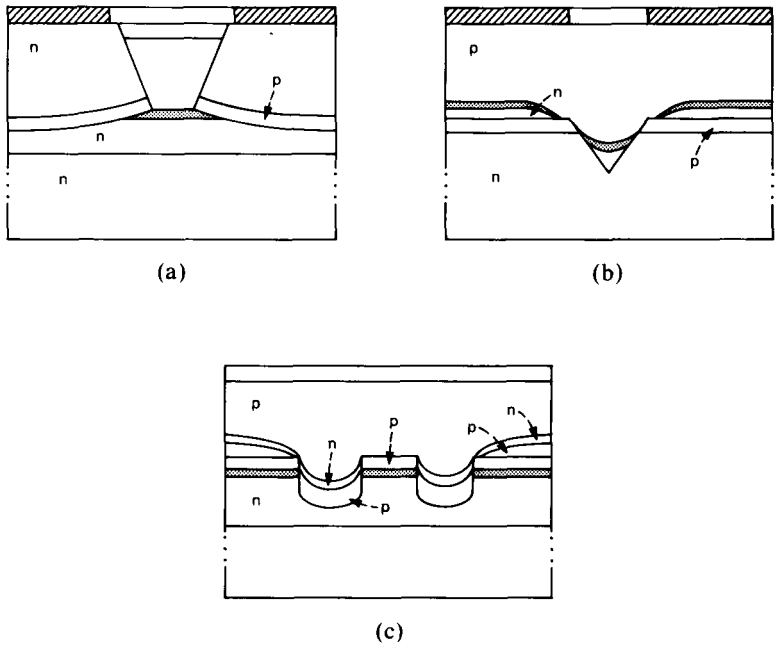

Fig. 9—The schematic cross sections of the (a) EMBH, (b) CSBH, and (c) DCPBH lasers are shown.

steps.[40] Briefly, a planar double heterostructure is grown by LPE over a n-InP substrate followed by the double channel etching and then regrowth. The CW light-current (L-I) characteristics of a DCPBH laser emitting at 1.3 μm is shown in Fig. 10. Note that this particular laser operates CW up to 130°C. These lasers typically have pulsed threshold currents in the range 15 to 25 mA at 30°C, and external differential quantum efficiencies in the range 0.2 to 0.25 mW/mA/facet. The variation of threshold current (I_{th}) with temperature (T) is given by the commonly used expression $I_{th}(T) \sim I_0 \exp(T/T_0)$, with T_0 values in the range 80 to 100K. The higher T_0 values of many DCPBH lasers when compared with broad area lasers ($T_0 \sim$ 60 to 70K) could be due to a small (~10 mA) temperature-independent leakage current. This is supported by our observation that lasers with low threshold (<15 mA at 30°C) have smaller T_0 values than lasers with somewhat higher threshold (~25 mA at 30°C).

Figure 11 shows the L-I characteristics of a DCPBH laser emitting at 1.55 μm. The doping levels and layer thicknesses of the lasers emitting at 1.55 and 1.3 μm are similar except that the 1.55-μm double heterostructure has an antimeltback layer (~0.15 μm thick) of 1.3-μm InGaAsP.

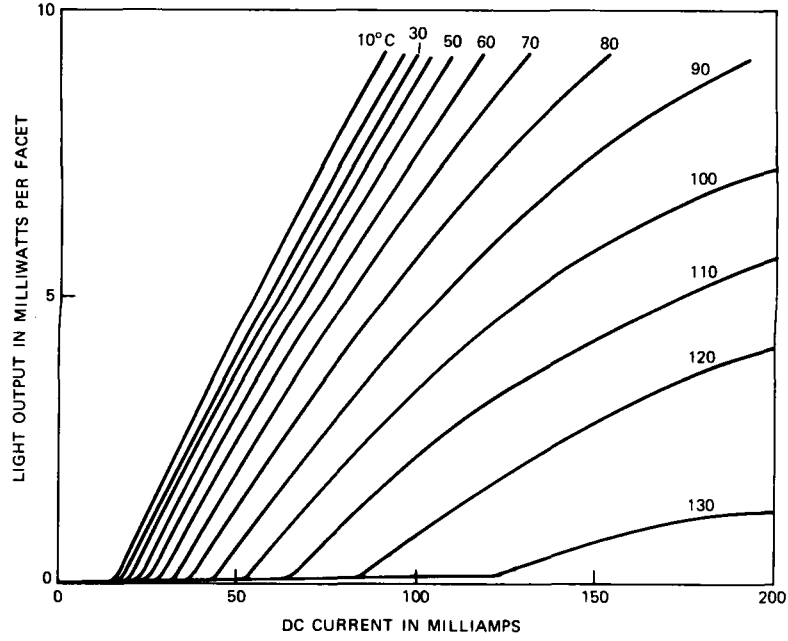

Fig. 10—Light-current characteristics of a DCPBH laser emitting at 1.3 μm.

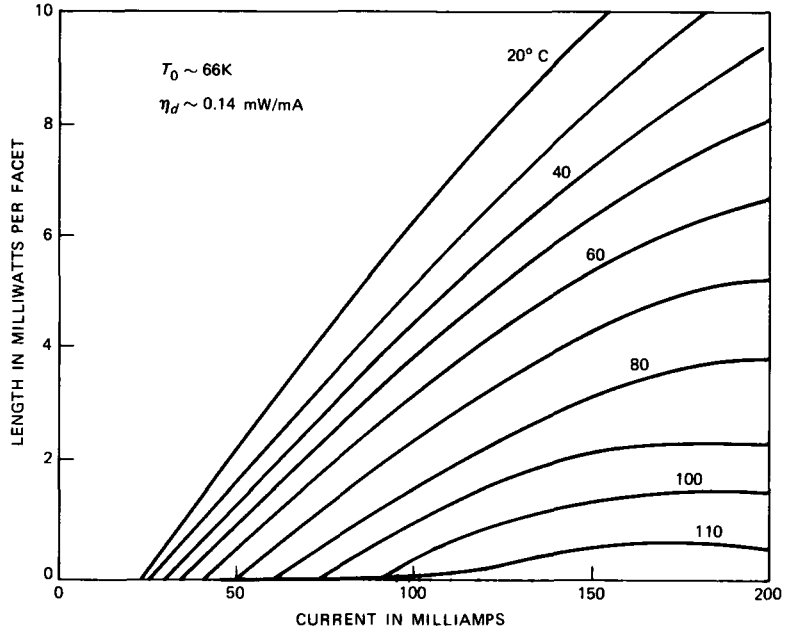

Fig. 11—Light-current characteristics of a DCPBH laser emitting at 1.55 μm.

Table II—Performance characteristics of typical DCPBH lasers

	$\lambda = 1.3$ μm	$\lambda = 1.5$ μm
I_{th} (30°C)	15–25 mA	20–35 mA
L(100 mA)	10–16 mW	6–9 mW
Efficiency/facet	0.2–0.25 mW/mA	0.12–0.15 mW/mA
T_0	90–100K	55–65K
T_{max} (CW)	130°C	110°C
Fabrication requirements		
Active area (kinks)	<0.3 μm^2	<0.2 μm^2
Antimeltback layer thickness (I_{th})	—	0.1–0.15 μm

The performance characteristics of our typical DCPBH lasers emitting at 1.3 and 1.5 μm are compared in Table II. The parameters shown are threshold current, external differential quantum efficiency, light output at 100 mA, T_0, and the maximum CW operating temperature (T_{max}). The performance of these lasers at both wavelengths are acceptable for many lightwave system applications. Nevertheless, we are interested in determining to what extent 1.3-μm lasers are intrinsically superior to 1.55-μm devices and to what extent the present differences represent relatively easy-to-overcome technological differences. The lowest threshold current observed for 1.3- and 1.55-μm lasers are 12 and 15 mA at 30°C. The maximum CW operating temperature of these lasers are 130 and 110°C, respectively.

The threshold current of the 1.5-μm lasers are slightly higher (~30 percent) than that for the 1.3-μm lasers. This is due to the smaller confinement factor of the waveguide mode of the lasers emitting at 1.5 μm caused by the antimeltback layer. This additional layer is not required for double heterostructures grown by vapor phase epitaxy, and hence in that case the threshold current may be lower.

The external differential quantum efficiency per facet of the lasers emitting at 1.55 μm is lower than that for lasers emitting at 1.3 μm. Using $\eta_d = 0.25$ mW/mA for 1.3-μm lasers and 0.15 mW/mA for 1.5-μm lasers, the optical absorption of the guided mode using eq. (4) is 37 and 67 cm^{-1} for the lasers emitting at 1.3 and 1.5 μm, respectively. In deriving the above, we have used a mirror loss of 40 cm^{-1}, which corresponds to a mode reflectivity of 0.35 for our 2.50-μm long lasers. The optical loss of the mode is related to the cladding and active layer loss by the following expression:

$$\alpha = \Gamma\alpha_a + (1 - \Gamma)\alpha_c. \tag{6}$$

Using $\alpha_c = 30$ cm^{-1} for both wavelengths and a calculated $\Gamma = 0.47$ and 0.38 for the 1.3- and 1.5-μm laser structure, we get $\alpha_a = 44$ and 127 cm^{-1} for the active layer losses of the 1.3- and 1.55-μm laser,

respectively, at 30°C. These estimates of the absorption loss are an upper limit because eq. (4) neglects the effect of leakage currents, which can reduce the efficiency. The external differential quantum efficiency can be increased by decreasing the length of the laser. For 1.55-μm lasers, a smaller confinement factor can also increase the efficiency, as discussed in Section IV.

The light output at 100 mA is also shown in Table II because it can be a measure of the combined effect of threshold current and external differential quantum efficiency and also provide an estimate of the drive current needed when the laser is used in lightwave transmitters. Note that this quantity is smaller for lasers emitting at 1.5 μm, because of the combined effect of lower efficiency and lower photon energy of these devices. Shorter lasers should have higher light output at 100 mA than that shown in Table II. However, the reliability of short lasers may be a problem because of higher threshold current (and carrier) density.

The observed temperature dependence of threshold current of lasers emitting at 1.3 μm is lower than that for lasers emitting at 1.5 μm. This is represented by higher T_0 value of the 1.3-μm lasers. We believe that a temperature-independent leakage path (leakage current ~10 mA at 30°C) can be responsible for high T_0 (~90 to 100K) of 1.3-μm lasers because low threshold (I_{th} ~ 15 mA at 30°C) 1.3-μm lasers have lower T_0 (~75K). High T_0 values caused by leakage current have been observed previously in EMBH lasers emitting at 1.3 μm.[43] The smaller leakage current in the DCPBH structure enables 1.3-μm DCPBH lasers to operate at temperatures as high as 130°C.

Spatial hole burning causes transverse mode transitions with increasing injection in strongly index-guided lasers.[44] These mode transitions appear as "kinks" in the *L-I* characteristics and are undesirable for lightwave applications. Spatial hole burning can be reduced and the *L-I* kinks eliminated by reducing the active area of the laser to less than ~0.3 μm^2 for lasers emitting at 1.3 μm[44] and ~0.2 μm^2 for lasers emitting at 1.55 μm. This fabrication requirement for kink-free operation of 1.55-μm lasers is more difficult to achieve.

6.2 Etched mesa buried heterostructure laser

The light-output-current characteristics of a EMBH laser emitting at 1.3 μm is shown in Fig. 12. These lasers typically have threshold current in the range 15 to 30 mA at 30°C and external differential quantum efficiency in the range 0.2 to 0.25 mW/mA. The lowest threshold current observed for 1.3-μm EMBH lasers is 11 mA at 30°C and the maximum CW operating temperature is 100°C. The variation of threshold current (I_{th}) with temperature (T) is given by T_0 values in the range 60 to 75K. These lasers with optimized layer thicknesses

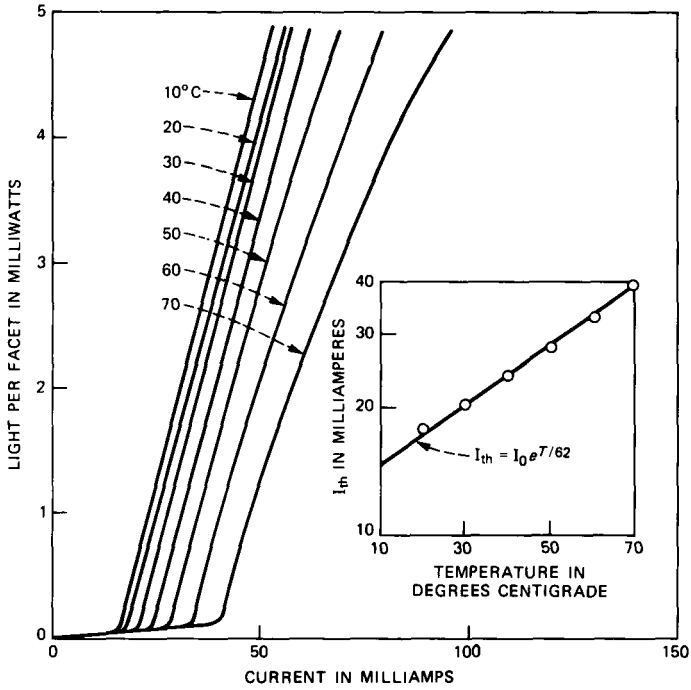

Fig. 12—Light-current characteristics of a EMBH laser emitting at 1.3 μm.

and doping levels do not exhibit a sublinearity in the light-current characteristics for power less than ~15 mW/facet near room temperature. At high injection, thyristor-like leakage path causes the *L-I* characteristics to roll over.[12,45] The fabrication requirements on active layer dimensions for low-threshold and kink-free operation of these lasers are shown in Table II.

6.3 Channeled substrate buried heterostructure lasers

We now discuss the experimental results for the CSBH laser (which has a nonplanar active layer). The schematic cross section of this device structure is shown in Fig. 9b. The light-current (*L-I*) characteristics of a CSBH laser emitting at 1.3 μm is shown in Fig. 13. The CSBH lasers are fabricated by LPE growth of an n-InP layer, 1.3-μm InGaAsP active layer, p-InP layer, and InGaAs contact layer over a base structure that has V grooves etched in it. The base structure has a p-InP current blocking layer, which may be LPE grown[37] or VPE grown[46] over an n-InP substrate. Cd-diffusion can also be used to form the blocking layer.[47] Alternatively, Fe implantation[48] or Fe-doped high-resistivity InP layers[49] can be used to limit the current flow to the active region in the V groove. All of the above schemes for base

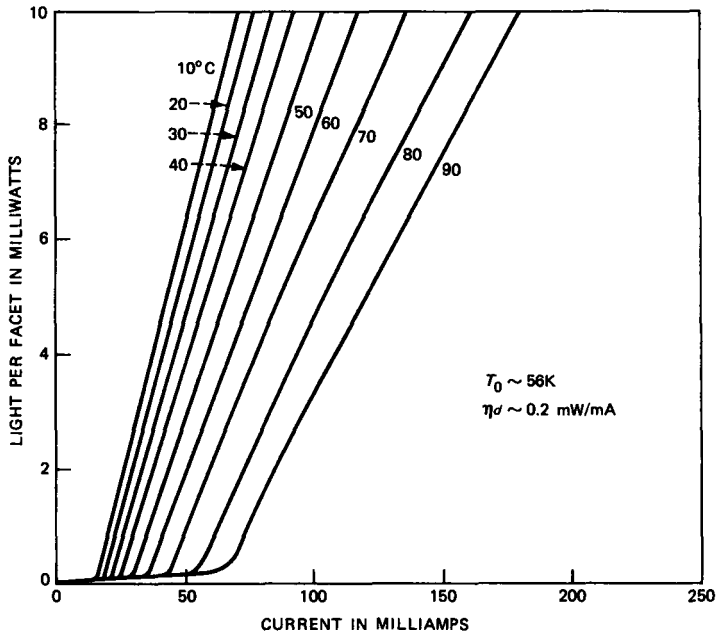

Fig. 13—Light-current characteristics of a CSBH laser emitting at 1.3 μm.

structures of CSBH lasers yield devices with comparable threshold current and efficiency. The threshold current of CSBH lasers emitting at 1.3 μm is typically in the range of 15 to 30 mA, and external differential quantum efficiency is 0.17 to 0.20 mW/mA/facet. Kink-free operation has been achieved to >24 mW/facet in lasers with active area less than 0.3 μm^2[50].

CSBH lasers emitting at 1.55 μm have been fabricated using Cd-diffused base structure and Fe-doped InP—grown by Metal Organic Chemical Vapor Deposition (MOCVD)—base structure. Figure 14 shows the *L-I* characteristics of a CSBH laser emitting at 1.55 μm with a Cd-diffused base structure. The CSBH lasers emitting at 1.55 μm have lower quantum efficiency than lasers emitting at 1.3 μm. The threshold current, quantum efficiency, and T_0 values of CSBH lasers emitting at 1.55 μm fabricated using Cd-diffused and MOCVD base structures are similar.

Performances of typical CSBH lasers emitting at 1.3 and 1.55 μm are compared in Table III. The parameters shown are threshold current, efficiency, light output at 100 mA, T_0, and maximum CW operating temperature. The data are representative of results from several wafers of each type. The observed lowest threshold currents for CSBH lasers emitting at 1.3 and 1.55 μm are 12 and 18 mA at

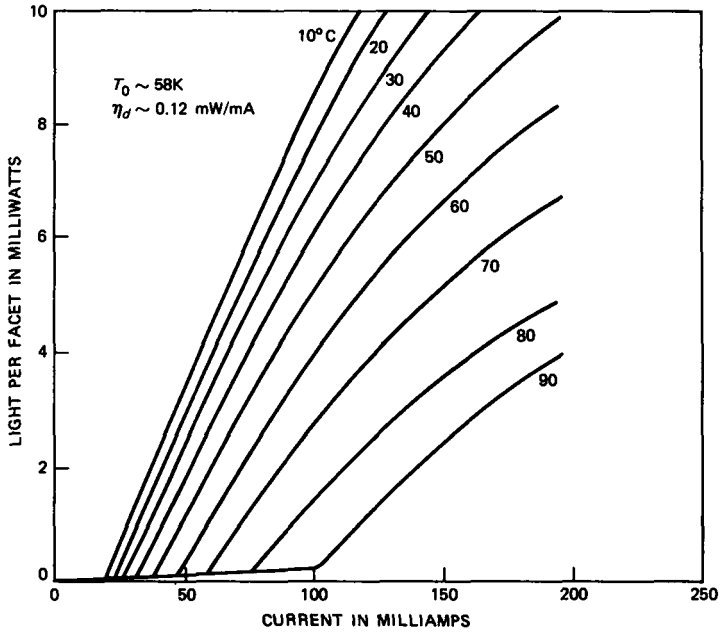

Fig. 14—Light-current characteristics of a CSBH laser emitting at 1.55 μm.

Table III—Performance characteristic of typical CSBH lasers

	$\lambda = 1.3$ μm	$\lambda = 1.5$ μm
I_{th} (30°C)	15–25 mA	25–35 mA
Efficiency/facet	0.17–0.2 mW/mA	0.11–0.14 mW/mA
L(100 mA)	8–13 mW	6–8 mW
T_0	50–55K	50K
T_{max}	90°C	90°C

30°C. The maximum CW operating temperatures for the 1.3- and 1.55-μm lasers are 120 and 90°C, respectively.

VII. DISCUSSION

The information-carrying capacity of a digital link is given by the product of the bit rate (B) and the distance (L) between the transmitter and the receiver. It is a common practice to characterize a transmission system by its bit-rate-distance product, although this may not be the judge of the overall performance.[51]

The loss limited transmission distance (L) is determined by the minimum number of photons per bit needed by a receiver to detect it. It is given by

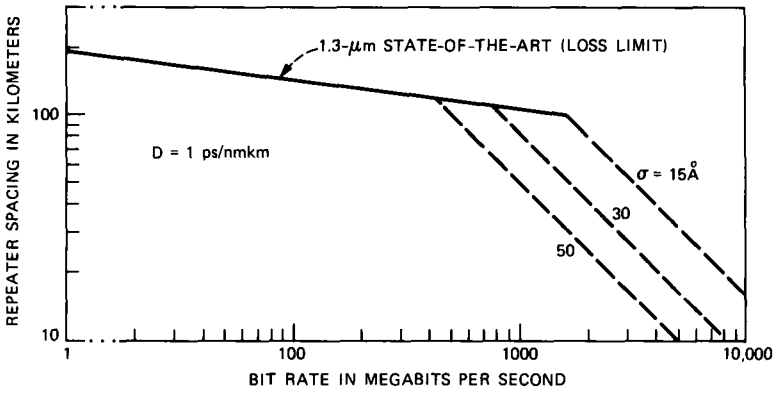

Fig. 15—Bit rate versus repeater spacing for lightwave systems operating near 1.3 μm.

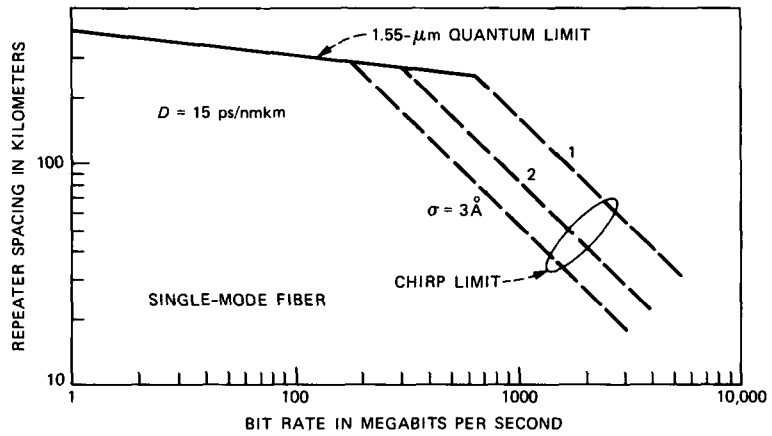

Fig. 16—Bit rate versus repeater spacing for lightwave systems operating near 1.55 μm.

$$P_R = P_T \exp(-\alpha L)$$

or

$$L = \frac{10}{\alpha} \log_{10} \frac{P_T}{P_R}, \tag{7}$$

where α is the fiber loss in dB/km and P_T, P_R is the transmitted and received power. For loss limit P_R varies linearly with the bit rate B. The solid lines in Figs. 15 and 16 show the loss limit for 1.3- and 1.55-μm systems using $P_T = 0$ dBm (1 mW).

At high bit-rate fiber dispersion becomes an important limitation because of pulse spreading. The effect of pulse spreading on the performance of lightwave systems have been calculated by several

authors.[52,53] The dispersion limit is usually given by[51] (within a factor of 2)

$$BL < 1/(AD\sigma), \tag{8}$$

where D is the fiber dispersion and σ is the source linewidth. Commercial silica fibers have zero dispersion near 1.3 μm and $D \sim 15$ ps/nmkm at 1.55 μm. Using $\sigma \sim 3$ nm for 1.55-μm multimode sources, eq. (8) suggests that in spite of the high loss limit the bit-rate-distance product is limited to 5.5 Gb-km for 1.55-μm transmission systems unless single-frequency sources are used.

Several schemes have been used to obtain single-frequency emission at 1.55 μm. Cleaved-coupled-cavity,[54] external cavity,[55] and DFB-type[42] single-frequency lasers have been fabricated using the DCPBH laser structure shown in Fig. 9c. Although all of these schemes produce essentially single-frequency sources (linewidth <20 MHz) under CW excitation, the linewidth under pulsed current modulation is significantly larger (1 to 2Å).[56-58] This phenomenon is usually called frequency chirping and it arises from a modulation of the refractive index by the injected current that modulates the effective cavity length. The chirp limit using eq. (8) for three different chirp widths is shown by the dashed curves in Fig. 16. External modulators must be used to eliminate the frequency chirping.

Dispersion limitations can also be important for 1.3-μm systems at high bit rates. In most optical fibers, the dispersion D is greater than 1 ps/nmkm at wavelength separation $\Delta\lambda > 10$ nm from the zero dispersion point. Using $D = 1$ ps/nmkm, we get the dashed lines in Fig. 15 as the dispersion limit for multimode source linewidths of 15, 30, and 50Å, respectively. The longitudinal mode spacing of a 2.50-μm long 1.3-μm InGaAsP laser is ~9Å. This suggests that the 30Å line in Fig. 9 may be a practical limit for 1.3-μm systems using multimode sources. Furthermore, it is well known that the emission spectrum of a 1.3-μm InGaAsP laser under microwave modulation (>2.5 Gb) is considerably broader (because of the appearance of many longitudinal modes) than for low bit-rate (<1 Gb) modulation.[59] This broadening is due to band filling, which becomes significant for modulation frequencies larger than inverse carrier recombination times. Thus, for high bit-rate-distance operation near 1.3 μm it is necessary to use single-frequency sources unless the emission spectrum under modulation is within ±10 nm of the zero dispersion wavelength of the fiber.

VIII. CONCLUSION AND SUMMARY

We have compared the performance of real index-guided InGaAsP lasers emitting at 1.3 and 1.55 μm. The 1.3-μm lasers have somewhat lower threshold current (~20 percent) than 1.55-μm lasers. This is

principally due to the smaller confinement factor of the 1.55-μm lasers due to the presence of the antimeltback layer in our LPE grown lasers. The VPE growth technique does not require the presence of antimeltbelt layer; thus essentially similar threshold current can be realized at both 1.3 and 1.55 μm. The measured median threshold current at 30°C from several wafers of our CSBH and DCPBH lasers are 15 to 25 and 20 to 35 mA for lasers emitting at 1.3 and 1.55 μm, respectively. The lowest threshold current observed at 30°C are 11 and 15 mA for lasers emitting at 1.3 and 1.55 μm, respectively.

The temperature dependence of the threshold current is given by the commonly used expression $I_{th}(\tau) \sim I_0 \exp(T/T_0)$ with T_0 ~60–75K for 1.3-μm lasers and 55- to 65K for 1.55-μm lasers. A small temperature-independent leakage current (~10 mA) is believed to be responsible for high T_0 values (~100K) of some 1.3-μm DCPBH lasers. The nonradiative Auger recombination process that increases with decreasing bandgap is believed to be responsible for the low T_0 values of the long-wavelength (both 1.3 and 1.55 μm) InGaAsP lasers. The effect of the larger Auger coefficient at 1.55 μm is compensated by lower carrier density at threshold at 1.55 μm so that the total nonradiative current loss for lasers emitting at 1.55 μm is not significantly larger than that for lasers emitting at 1.3 μm. This results in similar T_0 values for 1.3- and 1.55-μm lasers.

The measured efficiency of the 1.55-μm lasers is smaller (~20 percent) than that for 1.3-μm lasers. This may be due to the combined effect of larger intervalence band absorption and free carrier absorption at longer wavelengths. The smaller efficiency combined with lower photon energy (~20 percent) at 1.55 μm than at 1.33 μm makes the light output at a given operating current (~100 mA) of the 1.55-μm laser lower by ~35 percent than that for 1.3-μm lasers. This shows that the transmitter circuitry will need higher drive current when 1.55-μm lasers are used. The higher operating current may have some reliability implications. The external differential quantum efficiency for 1.55-μm lasers can be increased by fabricating short lasers. However, the reliability of short lasers may be a problem because of higher threshold current density in these devices.

Capacitance associated with leakage junctions is believed to influence the high frequency modulation capability of index-guided lasers that use reverse biased junctions for current confinement. We have fabricated 1.3- and 1.55-μm lasers that can be modulated at high bit rates (>2 Gb/s). The laser linewidth under modulation is found to be significantly broader than that under CW operation. The phenomenon is called frequency chirping and arises from the modulation of the carrier density that modulates the refractive index of the guided wave. The measured chirp width of the 1.55-μm laser is larger than that for

the 1.3-μm laser, because of the larger variation of refractive index with carrier density at longer wavelengths. The thickness of the antimeltback layer in our 1.55-μm lasers determines to some extent the measured chirp width; for example, lasers with larger antimeltback layer thickness have smaller confinement factor and hence have less chirp. If the laser is modulated at bit rates higher than the relaxation oscillation frequency, the chirp width is significantly enhanced. Since relaxation oscillations are damped in strongly index-guided lasers we expect these lasers to have less chirping at high bit rates (>1 Gb/s) than weakly index-guided lasers. The external cavity-type single-frequency lasers have been fabricated from our multimode lasers.[60] These single-frequency lasers exhibit less chirp (~2) than the multimode lasers due to frequency pulling effect.[61] Such frequency pulling effects can reduce the chirp width of distributed feedback type of lasers also. A chirp of 1Å limits the bit-rate distance product to 160 Gb-km for 1.55-μm transmission systems using conventional silica fibers.

REFERENCES

1. H. Kressel, Ed., *Semiconductor Devices for Optical Communication*, Berlin, New York: Springer-Verlag, 1980, Chap. 9.
2. S. E. Miller and A. G. Chynoweth, Ed., *Optical Fiber Telecommunication*, New York: Academic Press, 1979, Chaps. 1 and 21.
3. Y. Suematsu, "Long-Wavelength Optical Fiber Communication," Proc. IEEE, *71* (June 1983), pp. 692–721.
4. S. R. Nagel, K. L. Walker, and J. B. MacChesney, "Current Status of MCVD: Process and Performance," Tech. Dig. Topical Meeting Opt. Fiber Commun., Phoenix, Ariz., April 1982, Paper TuCC2.
5. R. A. Linke et al., "A 1 Gb/s Transmission Experiment Over 101 km of Single Mode Fiber Using a 1.55 μm Ridge Guide C^3-Laser," Electron. Lett, *20* (1984), pp. 472–4.
6. B. L. Kasper et al., "A 161.5 km Transmission Experiment at 420 Mb/s," Proc. Eur. Conf. Opt. Commun., Stuttgart, August 1984.
7. N. K. Dutta and R. J. Nelson, "The Case for Auger Recombination in InGaAsP," J. Appl. Phys., *53* (January 1982), pp. 74–92.
8. A. Sugimura, "Band to Band Auger Recombination Effect on InGaAsP Laser Threshold," IEEE J. Quantum Electron., *QE-17* (May 1981), pp. 627–35.
9. A. R. Adams et al., "The Temperature Dependence of the Efficiency and Threshold Current of InGaAsP Lasers Related to Intervalence Band Adsorption," Jap. J. Appl. Phys., *19* (October 1980), pp. L621–4.
10. K. Sakai, S. Akiba, and T. Yamamota, "InGaAsP Double Heterostructure Laser," Jap. J. Appl. Phys., *16* (1977), pp. 2043–5.
11. R. J. Nelson and N. K. Dutta, "Self Sustained Pulsations and Negative Resistance Behavior in InGaAsP Double Heterostructure Lasers," Appl. Phys. Lett., *37* (November 1980), pp. 769–71.
12. N. K. Dutta, D. P. Wilt, and R. J. Nelson, "Analysis of Leakage Currents in 1.3 μm InGaAsP Real-Index-Guided-Lasers," J. Lightwave Technol., *LT-2* (June 1984), pp. 201–8.
13. A. R. Beattie and P. T. Landsberg, "Auger Effect in Semiconductors," Proc. Roy. Soc. London, *249* (1959), pp. 16–28.
14. F. Stern, "Calculated Spectral Dependence of Gain in Excited GaAs," J. Appl. Phys., *47* (December 1976), pp. 5382–6.
15. N. K. Dutta, "Gain-Current Relation for InGaAsP Lasers," J. Appl. Phys., *52* (January 1981), pp. 55–60.
16. A. Mozer et al., "Losses in GaInAsP/InP and GaAlSb(As)/GaSb Lasers—The Influence of Split-Off Valence Band," IEEE J. Quantum Electron., *QE-19* (June 1983), pp. 913–6.

17. B. Sermage et al., "Photoexcited Carrier Lifetime and Auger Recombination in 1.3 μm InGaAsP," Appl. Phys. Lett., *42* (February 1983), pp. 259–61.
18. G. H. B. Thompson, "Analysis of Radiative and Nonradiative Recombination Law in Lightly Doped InGaAsP Lasers," Electron. Lett., *19* (March 1983), pp. 154–5.
19. T. Uji, K. Iwamoto, and R. Lang, "Nonradiative Recombination in InGaAsP-InP Light Sources Causing Light Emitting Diode Output Saturation and Strong Laser-Threshold-Current Temperature Sensitivity," Appl. Phys. Lett., *38* (February 1981), pp. 193–5.
20. G. P. Agrawal and N. K. Dutta, "Effect of Auger Recombination on the Threshold Characteristics of Gain Guided InGaAsP Lasers," Electron. Lett., *19* (November 1983), pp. 974–6.
21. C. B. Su et al., "Measurement of Radiative and Auger Recombination Rates in p-Type InGaAsP Diode Lasers," Electron. Lett., *18* (July 1982), pp. 595–6.
22. E. Winter and E. P. Ippen, "Nonlinear Carrier Dynamics in GaInAsP Compounds," Appl. Phys. Lett., *44* (May 1984), pp. 999–1001.
23. R. J. Nelson and N. K. Dutta, "Calculated Auger Rates and Temperature Dependence of Threshold for Semiconductor Lasers Emitting at 1.3 and 1.55 μm," J. Appl. Phys., *54* (June 1983), pp. 2923–9.
24. W. B. Joyce and R. W. Dixon, "Analytic Approximations for the Fermi Energy of an Ideal Fermi Gas," *31* (September 1977), pp. 354–6.
25. E. O. Kane, "Band Structure of Indium Antimoride," J. Phys. Chem. Solids., *1* (1957), pp. 249–61.
26. A. Haug, "Auger Recombination in InGaAsP," Appl. Phys. Lett., *42* (March 1983), pp. 512–4.
27. J. R. Chelikowsky and M. L. Cohen, "Nonlocal Pseudo Potential Calculation for the Electronic Structure of Eleven Diamond and Zinc-Blende Semiconductors," Phys. Rev., B, *14* (July 1976), pp. 556–82.
28. N. K. Dutta et al., "Temperature Dependence of Threshold Current of Injection Lasers for Short Pulse Excitation," Appl. Phys. Lett., *44* (May 1984), pp. 943–4.
29. N. K. Dutta, "Calculated Temperature Dependence of Threshold Current of GaAs-AlGaAs Double Heterostructure Lasers," J. Appl. Phys., *52* (January 1981), pp. 70–3.
30. P. J. Anthony and N. E. Schumaker "Ambipolar Transport in Double Heterostructure Injection Lasers," IEEE Electron Dev. Lett., *EDL-1* (April 1980), pp. 58–60.
31. B. Etienne et al., "Influence of Hot Carriers on Temperature Dependence of Threshold of InGaAsP Lasers," Appl. Phys. Lett., *41* (1982), p. 1018.
32. S. Yamakoshi et al., "Direct Observation of Electron Leakage in InGaAsP/InP Double Heterostructure," Appl. Phys. Lett., *40* (January 1982), pp. 144–6.
33. C. H. Henry et al., "Minority Carrier Lifetime and Luminescence Efficiency of 1.3 μm InGaAsP-InP Double Heterostructure Lasers," IEEE J. Quantum Electron., *QE-19* (June 1983), pp. 905–13.
34. C. H. Henry et al., "The Effect of Intervalence Band Absorption on the Thermal Behavior of InGaAsP Lasers," IEEE J. Quantum Electron., *QE-19* (June 1983), pp. 747–53.
35. J. K. Butler, "Theory of Transverse Cavity Mode Selection in Homojunction and Heterojunction Semiconductor Diode Lasers," J. Appl. Phys., *42* (October 1971), pp. 4447–57.
36. E. J. Flynn and D. A. Ackermann, unpublished work.
37. H. Ishikawa et al., "V-Grooved Substrate Buried Heterostructure InGaAsP/InP Laser With Smooth Far Field Pattern and Stable Aging Characteristics," Jap. J. Appl. Phys., *21*, Suppl. 21–1 (1982), pp. 435–6.
38. M. Hirao et al., "Fabrication and Characterization of Narrow Stripe InGaAsP/InP Buried Heterostructure Lasers," J. Appl. Phys., *51* (August 1980), pp. 4539–40.
39. R. J. Nelson et al., "CW Electrooptical Properties of InGaAsP (λ = 1.3 μm) Buried Heterostructure Lasers," IEEE J. Quantum Electron., *QE-17* (February 1981), pp. 202–7.
40. I. Mito et al., "InGaAsP Double Channel Planar Buried Heterostructure Lasers Diode (DCPBH-LD) With Effective Current Confinement IEEE," J. Lightwave Technol., *LT-1* (March 1983), pp. 195–202.
41. P. D. Wright et al., "Long Wavelength InGaAsP Lasers," Fiber Optic Communication/Local Area Network Conf., Atlantic City, N.J., October 10–14, 1983.
42. S. Akiba et al., "Low Threshold Current Distributed-Feedback InGaAsP/InP CW Lasers," Electron. Lett., *18* (January 1982), pp. 77–8.
43. N. K. Dutta et al., "InGaAsP Laser With Light T_0," IEEE J. Quantum Electron., *QE-18* (October 1982), pp. 1414–6.
44. N. K. Dutta et al., "Criterion for Improved Linearity of 1.3 μm InGaAsP-InP Buried

Heterostructure Lasers," IEEE J. Lightwave Technol., *LT-2* (April 1984), pp. 160–4.
45. F. R. Nash et al., "Implementation of the Proposed Reliability Assurance Strategy for an InGaAsP/InP, Planar Mesa, Buried Heterostructure Laser Operating at 1.3 μm for Use in a Submarine Cable," AT&T Tech. J., *64* (March 1985), pp. 809–60.
46. D. P. Wilt et al., "Channelled Substrate Buried Heterostructure Laser Using Hybrid VPE and LPE," J. Appl. Phys., *56* (August 1984), pp. 710–2.
47. H. Ishikawa et al., "V-Grooved Substrate Buried Heterostructure InGaAsP/InP Laser by One Step Epitaxy," J. Appl. Phys., *53* (April 1982), pp. 2851–3.
48. D. P. Wilt et al., "Channelled Substrate Laser Using Fe Implantation for Current Confinement," Appl. Phys. Lett., *44* (1984), pp. 290–3.
49. D. P. Wilt et al., unpublished work.
50. N. K. Dutta "Improved Linearity and Kink Criterion for 1.3 μm InGaAsP-InP Channelled Substrate BH Laser," Appl. Phys. Lett., *44* (March 1984), pp. 483–5.
51. P. S. Henry, unpublished work.
52. S. D. Personick, "Receiver Design for Digital Fiber Optic Communication System—Part I," B.S.T.J., *52* (July–August 1973), pp. 843–74.
53. J. E. Midwinter, *Optical Fibers for Transmission*, New York: Wiley, 1979, Chap. 8.
54. W. T. Tsang, N. A. Olsson, and R. A. Logan, "High Speed Direct Single-Frequency Modulation With Large Tuning Rate and Frequency Excursion in Cleaved Coupled Cavity Semiconductor Laser," Appl. Phys. Lett., *42* (March 1983), pp. 650–3.
55. K.-Y. Liou, "Single Longitudial Mode Operation of Injection Laser Coupled to a GRINROD External Cavity," Electron. Lett., *19* (1983), pp. 750–2.
56. N. A. Olsson, N. K. Dutta, and K-Y. Liou, "Dynamic Line Width of Amplitude Modulated Single Longitudinal Mode Semiconductor Lasers," Electron. Lett., *20* (February 1984), pp. 121–2.
57. N. K. Dutta et al., "Frequency Chirp Under Current Modulation in InGaAsP Injection Lasers," J. Appl. Phys., *56* (October 1984), pp. 2167–9.
58. K. Kishiuo, S. Aoki, and Y. Suematsu, "Wavelength Variation of 1.6 μm Wavelength Buried Heterostructure GaInAsP/InP Lasers Due to Direct Modulation," IEEE J. Quantum Electron., *QE-18* (1982), pp. 343–51.
59. F. Bosch, G. L. Dybwad, and C. B. Swan, U.S. Patent 4-317-236, February 1982.
60. N. A. Olsson et al., "2 Gb/s Operation of Single Longitudinal Mode 1.5 μm Double-Channel Planar Buried Heterostructure C^3 Lasers," Electron. Lett., *20* (May 1984), pp. 395–7.
61. G. P. Agrawal, N. A. Olsson, and N. K. Dutta, "Reduced Chirping in Coupled-Cavity Semiconductor Lasers," Appl. Phys. Lett., *45* (July 1984), pp. 119–21.

AUTHORS

P. Besomi, Ph.D. (Materials Science), 1982, Northwestern University; AT&T Bell Laboratories, 1981–1984; General Optronics, 1984—. Mr. Besomi is presently product line manager for InGaAsP LEDs and detectors.

Robert L. Brown, Certificate (Electrical Engineering), 1953, RCA Institute, N.Y.; AT&T Bell Laboratories, 1953—. Mr. Brown has worked on Si, GaAs, and InP devices. He is currently a Member of Technical Staff and is the author of 46 publications.

Richard W. Dixon, A.B. (Engineering and Applied Physics), 1958, Harvard College; M.S. and Ph.D. (Engineering and Applied Physics), Harvard University, in 1960 and 1964, respectively; AT&T Bell Laboratories, 1965—. Mr. Dixon is currently the Director of the Lightwave Devices Laboratory of AT&T Bell Laboratories.

Niloy K. Dutta, B.Sc. (Physics, Honours), 1972, and M.Sc. (Physics), 1974, St. Stephen's College, New Delhi, India; Ph.D. (Physics), 1978, Cornell Uni-

versity, Ithaca, N.Y.; AT&T Bell Laboratories, 1979—. Mr. Dutta was a Postdoctoral Associate at Cornell University for one and half years. During his doctoral and postdoctoral work at Cornell, he worked on spin-flip Raman lasers, infrared spectroscopy, soft X-ray lasers, and nonlinear optics with nonmonochromatic waves. Since 1979 he has been a Member of Technical Staff at AT&T Bell Laboratories, where he has contributed extensively to the research and development of InGaAsP semiconductor lasers. Mr. Dutta has authored or coauthored more than 80 publications on his work and one book on *Long Wavelength Semiconductor Lasers*, which is to be published. Senior Member, IEEE. Member, American Physical Society, Optical Society of America.

Ronald J. Nelson, B.A. (Physics), MacMurray College; M.S. and Ph.D., University of Illinois, Urbana; AT&T Bell Laboratories, 1976–1984; Lytel Inc., 1984—. At AT&T Bell Laboratories Mr. Nelson carried out studies of deep trap states in GaAlAs, interfacial recombination in GaAlAs-GaAs heterojunctions, and both radiative and nonradiative processes in GaAs material and laser devices. He was also involved in the fabrication and characterization of InGaAsP injection lasers. Mr. Nelson was appointed Supervisor of the Long Wavelength Device group in 1979. Member, American Physical Society.

Randall B. Wilson, B.S. (Physical Chemistry), 1975, University of California, Berkeley; Ph.D. (Chemistry), 1979, The Massachusetts Institute of Technology; AT&T Bell Laboratories, 1979–1984; Lytel Inc., 1984—. At AT&T Bell Laboratories Mr. Wilson was involved in studying the properties and LPE growth of III-V materials for long-wavelength device applications.

Daniel P. Wilt, B.A. (Mathematics and Physics), 1976, University of Southern California, University Park; Ph.D. (Applied Physics), 1981, California Institute of Technology, Pasadena; AT&T Bell Laboratories, 1981—. Mr. Wilt is currently pursuing research in the field of semiconductor lasers. He was appointed Supervisor of Lightwave Materials group in 1984. Member, Phi Beta Kappa, and Phi Kappa Phi.